J Mater Sci (2009) 44:5452–5458
DOI 10.1007/s10853-009-3735-x

Effect of abnormal grain growth on tensile strength of Al–Cu–Mg alloy friction stir welded joints

M. A. Safarkhanian · M. Goodarzi · S. M. A. Boutorabi

Received: 14 January 2009 / Accepted: 9 July 2009 / Published online: 14 August 2009

Abstract An Al-4.5%Cu-1.5%Mg aluminum alloy with a T4 temper was friction stir welded, and the effect of the abnormal grain growth on the tensile strength of joints was investigated. Abnormal grain growth usually happens during post weld heat treatment. It is found that the tensile strength and elongation of the heat-treated joint will increase significantly if this phenomenon completely happens in stir zone. On the other hand stable grains in the stir zone have no effect on the mechanical properties of heat-treated joint.

Introduction

Friction stir welding (FSW) is patented in 1991 by TWI [1]. Some important materials, such as Al, Mg, Ti, and Cu alloys, that have low fusion weldability, have been successfully welded by this technique. In particular, FSW has been used to join high-strength aluminum alloys, such as 2024, which are considered as alloys with very low weldability [2–6]. The basic concept of FSW is remarkably simple. A non-consumable rotating tool with a specially designed pin and shoulder is inserted into abutting edges of sheets or plates to be joined and traversed along the line of joint.

Based on microstructural characterization of grains and precipitates, for FSW three distinct zones are identified: (1) the stir zone (SZ), (2) the thermo mechanically affected zone (TMAZ), and (3) the heat affected zone (HAZ) [7]. The HAZ experiences a thermal cycle, but does not undergo any plastic deformation. For heat-treatable aluminum alloys, Mahoney et al. [8] defined the HAZ as a zone experiencing temperature rise above 250 °C. In this particular group of alloys, the HAZ retains the same grain structure as the parent material, but thermal exposure above 250 °C results in a significant coarsening of precipitates or development of precipitate free zones. Shukla and Baeslack [9] studied the orientation relationship and morphology of S phase in the HAZ of 2024-T3 aluminum alloy by TEM. They observed that rod-shaped S phase transforms to lath-shaped as a result of increasing heat input during FSW. When the base material is in the peak hardened condition the HAZ exhibits lowest hardness and strength, and the fracture in tensile test occurs usually in this zone [6].

Although the FSW process can eliminate the cracks and porosity associated with fusion welding of alloys, the softening problem of joints can be a non-acceptable problem. Accordingly, it is necessary to find out some effective remedial process to improve the tensile strength of joints further. To restore the strength of the joint, one option is to fully post weld heat treatment (PWHT) of the welded components. However, it has been shown that the fine grains in the SZ are not stable during solution treatment [10–19]. This kind of microstructural instability has been identified as abnormal grain growth (AGG). The AGG is a microstructural phenomenon in which some grains grow abnormally at the expense of finer matrix grains, and it generally happens when the normal grain growth has stopped [20].

Krishnan [10] showed that the SZ in FSW Al 6061-O exhibited coarsened grains after solution treatment at temperatures between 520 and 560 °C. Charit et al. [11] reported that the AGG results in a reduction of superplasticity of Al 7475 at or above 467 °C. Charit and Mishra [12] reported the same results for Al 2024 alloy at or above 470 °C. Chen et al. [13] have demonstrated that the lower

M. A. Safarkhanian · M. Goodarzi (✉) · S. M. A. Boutorabi
School of Metallurgy and Materials Science, Iran University of Science and Technology, Tehran, Iran
e-mail: mgoodarzi@iust.ac.ir

welding heat input (lower rotational speed or higher travel speed), the lower the grain size of the AGG in the Al 2219-O. Hassan et al. [14] examined stability of fine grains in the SZ of FSW Al 7010 during PWHT and concluded that the AGG initiates at the bottom of the SZ at 475 °C. Recently Charit and Mishra [15] reported that the heat index (ω^2/v ratio) more than the linear energy (ω/v ratio) affects AGG extent after solution treatment at 490 °C for 1 h. They showed that in the most FSW joints, the grains of SZ after PWHT become more stable, as a result of higher heat index.

Feng et al. [16] showed that not only the coarsening degree of grains, but also the tensile strength increases with increasing solution temperature during the PWHT of the 2219-O aluminum alloy. Liu et al. [17] showed that the AGG occurs in the same alloy during PWHT. They illustrated that the tensile strength of heat-treated joints without zigzag line, increases significantly in comparison with the heat-treated joints with zigzag line. Attallah and Salem [18] explained that the tensile strength falls off sharply due to AGG in FSW Al 2095 alloy. Chen et al. [19] investigated the effects of PWHT on the mechanical properties and found that the heat-treated joints of 2219-O aluminum alloy possess a lower elongation than the as-welded joints. There is no evidence for AGG in friction stir welded joints of pure aluminum and other alloys (such as Fe, Ti, and Cu alloys) in literature.

The above published literatures show that the AGG is related not only to the alloy composition, but also to the heat treatment temperatures and welding parameters. Based on the previous literatures it seems that the effects of AGG on the mechanical properties of FSW joints have not been investigated sufficiently. Then it is important to understand how AGG affects the mechanical properties of heat-treated joints in heat treatable aluminum alloys. In the present work, an Al-4.5%Cu-1.5%Mg or 2024 aluminum alloy is selected as the experimental material for FSW to reveal the effect of AGG on the mechanical properties of heat-treated joints.

Experimental procedure

The base material used in this study was a 5 mm thick 2024-T4 aluminum alloy plate, with chemical composition and tensile strength listed in Table 1. Base material was friction stir welded vertical to the rolling direction with two rotational speeds of 450 and 900 rpm and same travel speed of 25 mm/min. The threaded pin of the tool had a diameter of 6 mm and was 4.7 mm long. Shoulder was 18 mm in diameter and the tilt angle was set equal to 3°. After welding, the joints were cut into two parts, one part for PWHT and the other for as-welded examinations. The PWHT included solution and natural aging treatments. The solution treatment was carried out at 490 °C for 1 h, followed by quenching at 25 °C. Then after 100 h natural aging treatment, samples were prepared and the microstructure and mechanical properties were evaluated.

For preparing all samples, joints were cross-sectioned perpendicular to welding direction. The samples were examined by optical microscopy, scanning electron microscopy (SEM), and transmission electron microscopy (TEM). Cross-sections of metallographic specimens were polished with a diamond paste, etched with Tucker's reagent (15 mL hydrochloric acid, 5 mL nitric acid, 5 mL hydrofluoric acid, and 8 mL water) and examined by optical microscopy. For TEM observations thin discs were removed from the SZ in the plane normal to the welding direction. Samples were prepared by jet electro-polishing in a nitric acid (30%) and methanol (70%) at −25 °C and 18 V. Microstructural investigations were carried out by a Philips CM200 instrument operating at 200 kV. The room temperature tensile test was carried out at a crosshead speed of 3 mm/min using an Instron 8500 testing machine. Stir zone strain during tensile test was measured by 2620-601 dynamic strain gage extensometer of Instron Company with 25 mm gage length. Tensile properties of each joint were evaluated using three specimens from the same joint. Fracture features of tensile specimens were analyzed by SEM. Vickers microhardness (H_v) measurements were also carried out at mid thickness and across the welded joints, using a Buehler 1600-4600 microhardness tester (100 gf load).

Results and discussion

Figure 1 shows the hardness distributions at mid thickness of the joints before and after PWHT. As seen the hardness of SZ, TMAZ and HAZ in as-welded joints decreased relative to the base metal. The softening is completely restored by PWHT. The softening of the HAZ in the

Table 1 ω chemical composition and tensile strength of 2024-T4 aluminum alloy plate

Chemical composition, wt%							Mechanical properties		
Al	Cu	Mg	Mn	Fe	Si	Zn	Tensile strength	0.2% proof strength	Elongation
Bal.	4.43	1.48	0.72	0.26	0.11	0.2	450 MPa	320 MPa	9%

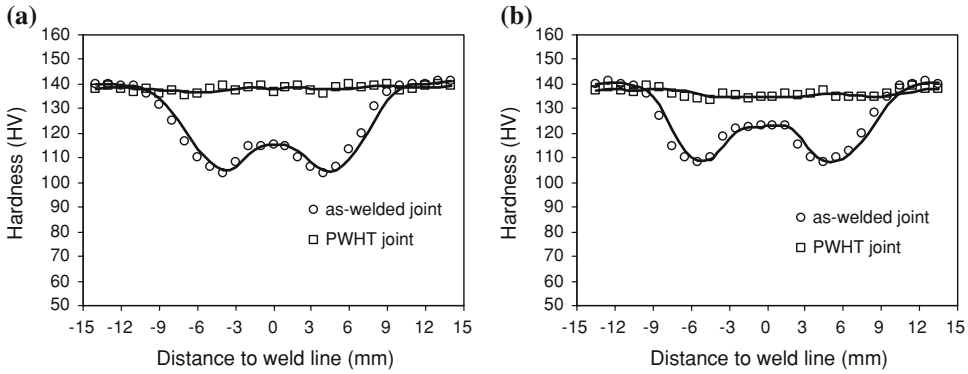

Fig. 1 Microhardness profile at mid thickness of the joints before and after PWHT; **a** $\omega = 450$ rpm **b** $\omega = 900$ rpm

as-welded joints can be attributed mainly to the dissolving or the coarsening of precipitates resulted from the thermal history during FSW. The higher hardness observed in the SZ and TMAZ can be attributed to the increase of volume fraction of the dissolved precipitates that increased the contents of alloying elements (in-solution) available for the precipitation hardening during natural aging [6]. The fully precipitation hardening after FSW led to removing the softening of these zones.

Figure 2 shows the tensile strength and elongation of joints and the base metal. As seen the ultimate strengths, yield strengths and elongations of as-welded joints, are about 12, 20, and 60% lower than the base metal, respectively. The PWHT joints exhibit significantly different mechanical properties. The tensile strength and elongation of the PWHT 900 rpm joint are almost the same as as-welded joints. However, the ultimate strength and elongation of the PWHT 450 rpm joint increase approximately 10 and 66%, respectively, by comparison with the base metal, even though yield strengths of this joint and the base metal are the same.

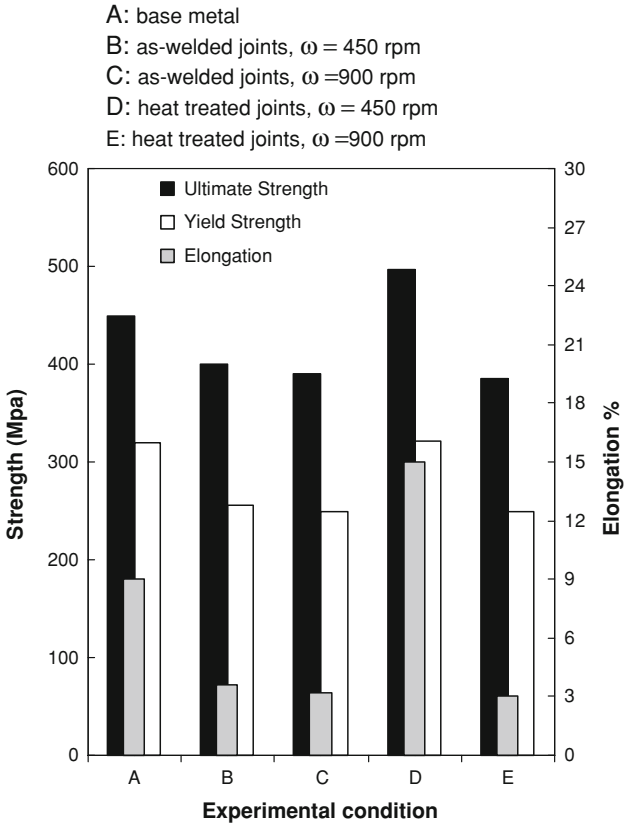

Fig. 2 Tensile strength of the base material and FSW joints

These results indicate that the tensile strength together with elongation have been increased by the PWHT only at special conditions. The macrostructure and fracture location of heat-treated joints are shown in Fig. 3. The AGG is observed in whole SZ of the joint with lower rotational speed (Fig. 3a), whilst this phenomenon is seen only at top and bottom of the joint with higher rotational speed (Fig. 3c). It can be concluded that AGG can increase the ductility along with strength values of the joint in comparison with the as-welded joint.

As seen in Fig. 3b, d, fracture location in heat-treated joints is in the SZ. The fracture faces of heat-treated joints, Fig. 4, exhibit a complete dimple structure. The depth and width of the observed dimples in fracture face of heat-treated 450 rpm joint are more, compared with heat-treated 900 rpm joint. It has been proved that the fracture energy does increase with increasing depth and width of the dimples [21]. Consequently the heat-treated 450 rpm joint is stronger than heat-treated 900 rpm joint.

The presence of AGG in the SZ has a significant effect on tensile strength of the heat-treated joint. This might be related to different microstructure characteristics in the SZ before and after PWHT.

As shown in Fig. 5 there are two different particles in as-received alloy, marked by A and B. The Energy-Dispersive Spectrometry (EDS) analysis showed that these particles are compounds of Al–Mg–Cu and Al–Cu–Fe–Mn (Fig. 5d, e). According to the literature these compounds are most likely Al_2CuMg and $(Cu,Fe,Mn)Al_6$ [22, 23]. Also it is shown that the large particles in the base metal (Fig. 5a) have been broken up to relatively small particles

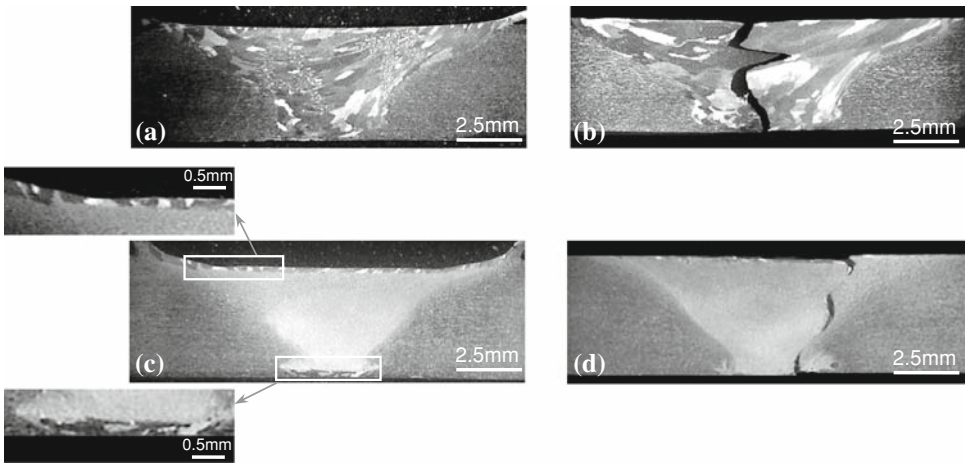

Fig. 3 Cross-section and fracture location of heat-treated joints: **a** and **b** $\omega = 450$ rpm; **c** and **d** $\omega = 900$ rpm

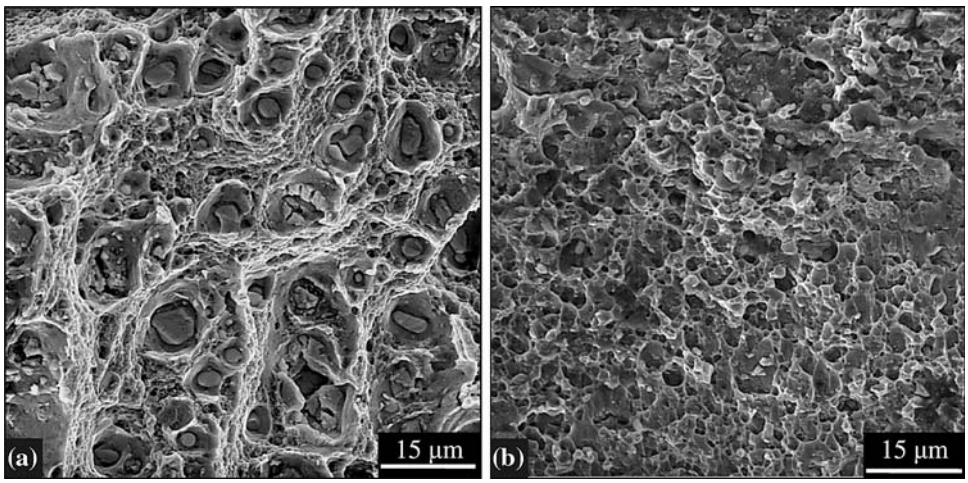

Fig. 4 Fracture feature of heat-treated FSW joints; **a** $\omega = 450$ rpm **b** $\omega = 900$ rpm

and the severity of breaking up of these particles in the stir zone increases with increasing rotational speed during FSW (Fig. 5b and c). Gerlich et al. [24] showed that rod-like Al_2CuMg precipitates in the Al 2024-T3 are broken up during friction stir spot welding. It is well known that severe plastic deformation during FSW is the main reason for breaking up of particles [25–27].

Figure 6 shows the grains and particles in the SZ of the as-welded 900 rpm joint. The grains in the SZ of the joint are fine and equiaxed. It is suggested that, during the FSW process, the dynamic recrystallization is responsible for production of new fine grains in the SZ [28–30]. Whereas the recrystallization occurs simultaneously with breaking up of particles during FSW, it is likely that the most of particles are located at the grain boundaries in the SZ of as-welded joints (Fig. 6). These particles remain at locked grain boundaries after PWHT (Fig. 7). While the AGG phenomenon is happening, the grain boundaries pass the pining particles and after that, particles do not locate at AGG grain boundaries. Figure 8a does not show any particles in AGG grain boundary for PWHT 450 rpm joint. However in Fig. 8b it is clear that particles remain at the non growing grain boundaries for the PWHT 900 rpm joint.

The problem of softening of the as-welded joints is eliminated by the PWHT, but another problem appears, that is weakening of the SZ because of locating of broken particles at the grain boundaries. The AGG causes these particles to locate inside the new grains, which result in increasing the tensile strength along with elongation values of heat-treated joint. However, Attallah and Salem [18] reported that AGG decreases the tensile strength in Al 2095 alloy, and Chen et al. [19] stated that it decreases the elongation of heat-treated joints in Al 2219 alloy.

Initial oxide layer on the butt surface fragments during FSW often remains as a faint zigzag-line pattern on the cross section. It has been reported that zigzag line produced by the low heat-input parameters (low rotational speed and high travel speed) [31, 32]. Liu et al. [17] explained that the zigzag line decreases the mechanical properties after PWHT.

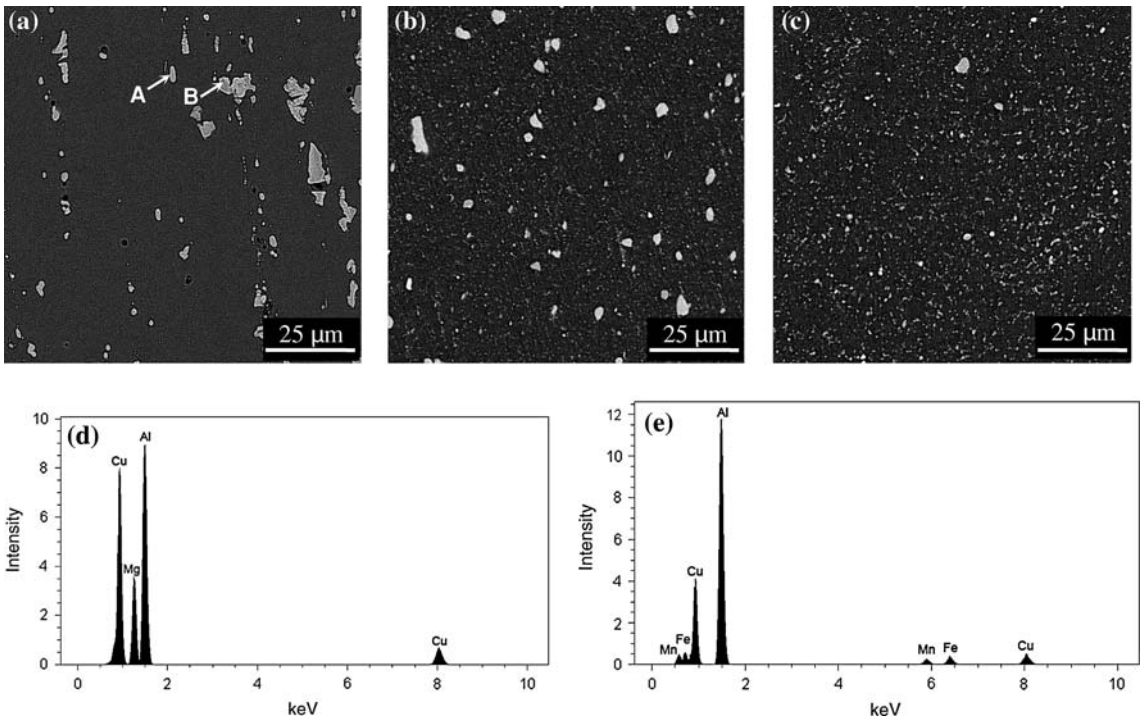

Fig. 5 Back scattered SEM images; **a** the base metal **b** the SZ in 450 rpm joint **c** the SZ in 900 rpm joint **d** EDS spectra of the A particle **e** EDS spectra of the B particle

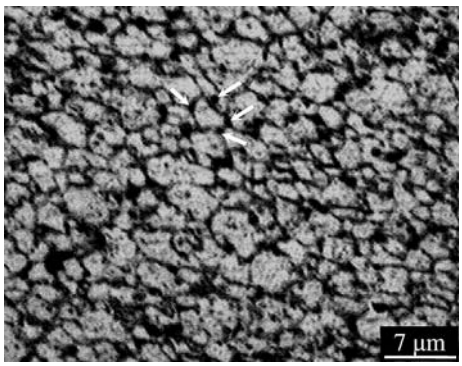

Fig. 6 Optical micrograph of the as-welded 900 rpm joint showing that broken particles are located at new grain boundaries (see *arrow*)

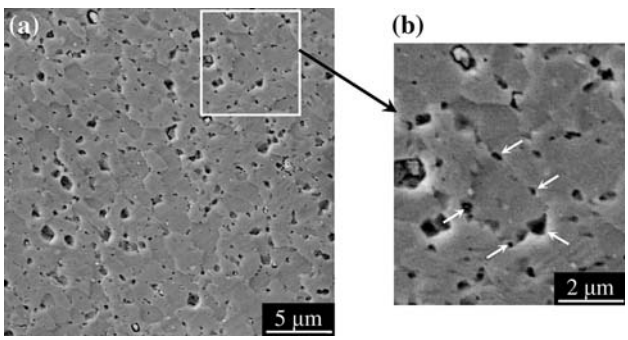

Fig. 7 Secondary electron SEM images of the SZ in the PWHT 900 rpm joint; **a** broken particles are mostly located at the grain boundaries, **b** same particles in higher magnification

A numerical three-dimensional heat flow model for friction stir welding of age hardenable aluminum alloy has been developed by Frigaard et al. [33], based on the finite difference scheme. According to their research the average heat input per unit time generated by the FSW process can be explained as Eq. 1.

$$Q = \frac{4}{3}\pi^2 PR^3 \mu\omega \tag{1}$$

where P is the vertical pressure on the tool (P_a), R surface radius of shoulder (m), μ friction coefficient, and ω is the tool rotation speed (rotations/s). Consequently the heat input per unit length during FSW can be expressed as Eq. 2.

$$q = \left(\frac{4}{3}\pi^2 PR^3 \mu\right)\frac{\omega}{v} = K\frac{\omega}{v} \tag{2}$$

where v is the welding speed (m/s). It can be supposed that P and μ do not vary during FSW, so that K value remains constant. According to Eq. 2, the FSW heat input (q) is proportional to welding parameter of ω/v.

The parameter of ω/v in of Attallah and Salem [18] and Chen et al. [19] investigations are significantly lower than that in the present study (Table 2). They used low heat input for welding procedure. It is likely that the lower mechanical properties reported by Attallah and Salem [18] and Chen et al. [19] were related to the formation of zigzag line defect at low heat input during FSW. In this study there are not any Zigzag line defects because the ω/v ratio

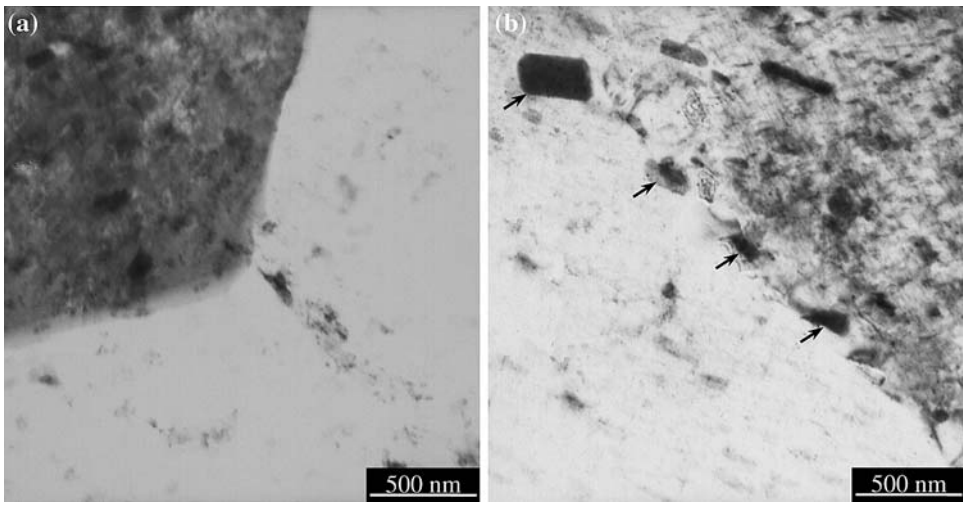

Fig. 8 TEM images of PWHT joints; **a** with AGG and $\omega = 450$ rpm, particles locate inside grains **b** without AGG and $\omega = 900$ rpm, particles mostly remain at grain boundaries (see *arrow*)

Table 2 Comparison of the ω/v value in this study with the ω/v value in the literature

	Alloy	ω (rpm)	v (mm/min)	ω/v (r/mm)
Attallah and Salem [18]	Al 2095	500–1000	126–306	1.6–7.9
Chen et al. [19]	Al 2219	800	100–400	2–8
This study	Al 2024	450–900	25	18–36

Table 3 Volume fraction and average diameter of particles and average radius of grains

	F_v	d (μm)	R (μm)	Z
$\omega = 450$ rpm	0.078	0.252	0.9	0.83
$\omega = 900$ rpm	0.12	0.13	2.02	5.78

is very high (Table 2), consequently the heat input is very high during FSW (Eq. 2). Therefore, zigzag line defect could not be produced in the SZ of the samples. Whereas the most of particles are located inside grains, during AGG phenomenon, it seems that the cause of increasing the strength and elongation values of the heat-treated joints is AGG.

The driving force for AGG, that is similar to normal grain growth, is to reduce the grain boundary energy and to achieve a more stable state. On the other hand the AGG is prevented by fine precipitates and particles. Humphreys and Hatherly [20] explained that AGG is possible when the pinning parameter, Z, is between 0.25 and 1 ($Z = 3F_vR/d$, where F_v is volume fraction of particles, R is average grain radius, and d is average particle diameter). However, based on Humphreys' model, the grain growth does not occur when $Z > 1$.

It is known that strengthening precipitates such as rod or lath shaped Al_2CuMg can only be seen by TEM at high magnification [9] and they dissolve completely during solution treatment. Therefore these precipitates do not play any role in initiation of AGG phenomenon during PWHT. As mentioned previously, there are two types of particles in the microstructure of as-received Al 2024. The Al_2CuMg particles, which are seen in microstructure after PWHT by SEM at low magnification, did not dissolve during solution treatment. They are soluble particles that do not dissolve during PWHT [34]. Also it is shown that particles, including Fe and Mn, are insoluble in aluminum alloys. Therefore $(Cu,Fe,Mn)Al_6$ particles are insoluble [34]. Consequently all particles, which can be seen in SEM image after PWHT are undissolved Al_2CuMg and insoluble $(Cu,Fe,Mn)Al_6$ particles that have major influence in the initiation of AGG phenomenon. Volume fraction and average diameter of the particles after PWHT and average radius of grains in as-welded condition are measured by an image analyzer. Table 3 shows that Z value is between 0.25 and 1 for as-welded 450 rpm joint while it is higher than 1 for as-welded 900 rpm joint. Therefore, the AGG takes place only for 450 rpm joint during PWHT.

Conclusions

(1) The softening of as-welded joints is completely eliminated by PWHT.
(2) The Al_2CuMg and $(Cu,Fe,Mn)Al_6$ particles in 2024-T4 alloy are broken up during FSW in the SZ. Severity of breaking up of these particles increases with increasing rotational speed. The most of the broken particles locate at the SZ grain boundaries.
(3) The broken particles are located inside grains after AGG, thus this phenomenon has a beneficial effect on tensile strength of the heat-treated FSW joint.

(4) Remaining of the broken particles at the grain boundaries that they do not growth abnormally during PWHT, decreases the tensile strength and elongation values.
(5) At the present study there are not any zigzag line defects because the value ω/v or heat input is high enough for welding process.
(6) The initiation of AGG during PWHT at present study obeys Humphreys' model and relates to average primary grain size, average undissolved or insoluble particles diameter, and volume fraction of these particles.

References

1. Thomas WM, Nicholas ED, Needham JC, Murch MG, Temple-Smith P, Dawes CJ (1991) International Patent Application PCT/GB92, Patent Application GB9125978.8, 6
2. Sutton MA, Yang B, Reynolds AP, Taylor R (2002) Mater Sci Eng A 323:160
3. Genevois C, Deschamps A, Denquin A, Doisneau-cottignies B (2005) Acta Mater 53:2447
4. Jones MJ, Heurtier P, Desrayaud C, Montheillet F, Allehaux D, Driver JH (2005) Scr Mater 52:693
5. Genevois C, Fabrègue D, Deschamps A, Poole WJ (2006) Mater Sci Eng A 441:39
6. Khodir SA, Shibayanagi T (2008) Mater Sci Eng B 148:82
7. Mishra RS, Ma ZY (2005) Mater Sci Eng R 50:1
8. Mahoney MW, Rhodes CG, Flintoff JG, Spurling RA, Bingel WH (1998) Metall Mater Trans 29A:1955
9. Shukla AK, Baeslack WA (2009) J Mater Sci 44:676. doi:10.1007/s10853-008-3212-y
10. Krishnan KN (2002) J Mater Sci 37:473. doi:10.1023/A:1013701104029
11. Charit I, Mishra RS, Mahoney MW (2002) Scr Mater 47:631
12. Charit I, Mishra RS (2003) Mater Sci Eng A 359:290
13. Chen YC, Feng JC, Liu HJ (2007) Mater Charac 58:174
14. Hassan KhAA, Norman AF, Price DA, Prangnell PB (2003) Acta Mater 51:1923
15. Charit I, Mishra RS (2008) Scr Mater 58:367
16. Feng JC, Chen YC, Liu HJ (2006) Mater Sci Technol 22:86
17. Liu HJ, Chen YC, Feng JC (2006) Scr Mater 55:231
18. Attallah MM, Salem HG (2005) Mater Sci Eng A 391:51
19. Chen YC, Liu HJ, Feng JC (2006) J Mater Sci 41:297. doi:10.1007/s10853-005-0640-9
20. Humphreys FJ, Hatherly M (2004) Recrystallization and related annealing phenomena, 2nd edn. Elsevier, New York
21. Hertzberg RW (1995) Deformation and fracture mechanics of engineering materials, 4th edn. Wiley, Hobokon
22. Mondolfo LF (1976) Aluminum alloys: structure and properties. Butterworth, London
23. Brooks CR (1984) Heat treatment, structure and properties of nonferrous alloys. ASM, Metals Park, OH, USA
24. Gerlich A, Su P, Yamamoto M, North TH (2007) J Mater Sci 42:5589. doi:10.1007/s10853-006-1103-7
25. Ma ZY, Sharma SR, Mishra RS (2006) Mater Sci Eng A433:269
26. Ma ZY, Sharma SR, Mishra RS (2006) Scr Mater 54:1623
27. Feng AH, Ma ZY (2007) Scr Mater 56:397
28. Etter AL, Baudin T, Fredj N, Penelle R (2007) Mater Sci Eng A 445–446:94
29. Salem HG (2003) Scr Mater 49:1103
30. Jata KV, Semiatin SL (2000) Scr Mater 43:743
31. Zhou C, Yang X, Luan G (2006) J Mater Sci 41:2771. doi:10.1007/s10853-006-6337-x
32. Sato YS, Takauchi H, Hwan S, Park C, Kokawa H (2005) Mater Sci Eng A 405:333
33. Frigaard Ø, Grong Ø, Midling OT (2001) Metall Mater Trans 32A:1189
34. Cravetchi IV, Taschuk M, Tsui YY, Fedosejevs R (2004) Spectrochim Acta B 59:1439